AGU PUBLICATIONS

Geophysical Research Letters

RESEARCH LETTER
10.1002/2015GL067288

Key Points:
- Innovative combination of oxygen isotope fractionation to understand crystallization kinetics
- Oxygen isotope change in quartz and alkali feldspar with position across spherulites
- Spherulites self-contain a record of their thermal history and crystallization

Supporting Information:
- Texts S1 and S2, Figures S1 and S2, and Caption for Table S1
- Table S1

Correspondence to:
K. Befus,
Kenneth_Befus@Baylor.edu

Citation:
Befus, K. S. (2016), Crystallization kinetics of rhyolitic melts using oxygen isotope ratios, *Geophys. Res. Lett.*, *43*, doi:10.1002/2015GL067288.

Received 3 DEC 2015
Accepted 3 JAN 2016
Accepted article online 6 JAN 2016

Crystallization kinetics of rhyolitic melts using oxygen isotope ratios

Kenneth S. Befus[1]

[1]Department of Geology, Baylor University, Waco, Texas, USA

Abstract Crystals provide the means to understand igneous systems, but natural constraints on crystallization kinetics are rare because thermal conditions and crystallization timescales are typically unknown. Oxygen isotope ratios in quartz and alkali feldspar crystals in spherulites provide a natural record of the temperature interval of crystallization and crystal growth rates in rhyolitic melts. Oxygen isotope compositions in both phases change progressively with position from the spherulite core to rim. Quartz $\delta^{18}O$ increases from 5.0 ± 0.3‰ in the core to 5.6 ± 0.3‰ at the rims, whereas alkali feldspar decreases from 3.7 ± 0.4‰ in the core to 2.7 ± 0.9‰ at the rims. Fractionation therefore increases from 1.3 ± 0.7‰ in the cores to 2.9 ± 1.1‰ at the rims. Oxygen isotope thermometry tracks crystallization temperature with position. Spherulites nucleate at 578 ± 160°C and continue to grow until 301 ± 88°C. The in situ analyses demonstrate that spherulites self-contain a record of their thermal history and that of the host lava.

1. Introduction

Crystals and crystal textures are the primary tools for understanding the storage conditions, crystallization ages, and emplacement of their host igneous systems. Crystal nucleation and growth occurs in response to undercooling, which can be produced by cooling, changing melt composition, or degassing. Natural constraints on growth and nucleation kinetics are rare and difficult to extract because the timing and thermal conditions of those systems are typically unconstrained. Thus, much of the community's understanding of crystallization is derived from experiments in which timescales and thermal conditions are carefully controlled [*Tuttle and Bowen*, 1958; *Yoder and Tilley*, 1962; *Cashman*, 1990; *Hammer and Rutherford*, 2002]. Using experimental techniques to draw parallels to natural systems has limitations; hence, kinetic information extracted from natural systems, such as the Makaopuhi lava lake and crystal size distributions of other systems, is noteworthy [*Kirkpatrick*, 1977; *Cashman and Marsh*, 1988; *Marsh*, 1988; *Cashman*, 1992].

A number of studies over the past decade have demonstrated that spherulites may naturally preserve a record of the crystallization and thermal history of lavas [*Castro et al.*, 2008, 2009; *Seaman et al.*, 2009; *Watkins et al.*, 2009; *Gardner et al.*, 2012; *von Aulock et al.*, 2013; *Befus et al.*, 2015]. Spherulites are spherical to ellipsoidal bodies of radiating, intergrown crystals (Figure S1 in the supporting information) that form by rapid crystallization of melt or glass in response to significant undercooling (ΔT), which is the temperature difference between the phase liquidus and crystal growth [*Keith and Padden,* 1963, 1964; *Lofgren*, 1971a, 1971b; *Castro et al.*, 2008; *Watkins et al.*, 2009; *Gardner et al.*, 2012; *Befus et al.*, 2015]. Spherulites have fascinated field geologists and experimental petrologists for well over a century [e.g., *Cross*, 1891; *Lofgren,* 1971a, 1971b]. They are common devitrification features in volcanic glasses from most volcanic environments. Spherulites are especially abundant in rapidly cooled portions of rhyolite lavas and welded ignimbrites. A review of spherulite textures and their geologic implications is provided by *Breitkreuz* [2013].

During spherulite growth incompatible elements are expelled into the surrounding matrix, producing incompatible element gradients [*Castro et al.*, 2008; *Watkins et al.*, 2009; *Gardner et al.*, 2012]. Numerical advection-diffusion models suggest those incompatible element gradients provide a record of nucleation and crystal growth and constrain spherulite nucleation to an interval of 700 to 500°C in a lava cooling at ~$10^{-5.2 \pm 0.3}$ °C s^{-1}, with growth ongoing to temperatures as cool as ~400°C [*Gardner et al.*, 2012; *Befus et al.*, 2015]. Max growth rates were estimated to be ~1 μm h^{-1}, which exponentially decreased with time. Those modeling estimates depend upon the complex interplay of numerous variables, including nucleation temperature, spherulite growth rate, growth law, lava cooling rate, element partitioning, and element diffusivity. Some of those variables are interdependent (e.g., temperature and diffusivity), whereas others have significant uncertainty. Thus, those models provide limited independent constraints.

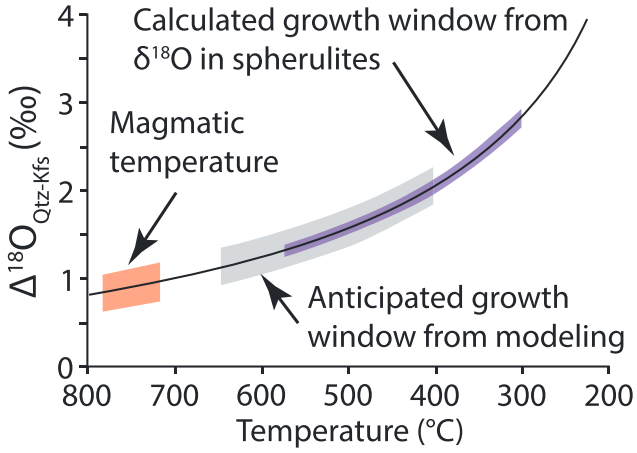

Figure 1. Oxygen isotope fractionation between quartz and alkali feldspar plotted against temperature, using the experimental data from *Clayton et al.* [1989]. The arrowed domains show the magmatic temperature of Pitchstone Plateau flow [*Befus,* 2014; *Stelten et al.,* 2015], the anticipated window of spherulite growth from past numerical modeling [*Gardner et al.,* 2012; *Befus et al.,* 2015], and these new results.

In situ oxygen isotope analyses of the crystalline phases in spherulites may provide an independent test for those models and provide exciting new, natural constraints on the crystallization kinetics and thermal conditions of rhyolite melts. Oxygen isotope fractionation between quartz and alkali feldspar is temperature dependent and is predicted to be <1‰ at temperatures >700°C, but increases with decreasing temperature (Figure 1) [*Zheng*, 1993]. Quartz and alkali feldspar phenocrysts typically record small fractionations consistent with crystallization at magmatic temperatures [*Bindeman and Valley*, 2001], whereas lower temperature hydrothermal or metamorphic crystallization would produce fractionations that can be used reliably as an isotopic thermometer [*Matsuhisa et al.*, 1979; *Matthews*, 1994]. If spherulites nucleate and grow over the interval of 700 to 400°C as modeling results suggest, then fractionation values in spherulites should be greater than 1‰ and increase toward spherulite rims.

This study was designed to take advantage of this unique opportunity to exploit oxygen isotope fractionation to understand natural crystallization kinetics. To test if spherulites self-contain a record of their thermal history, I use in situ spot analyses to measure the oxygen isotope compositions ($\delta^{18}O$) and fractionation between quartz and alkali feldspar ($\Delta^{18}O_{Qtz\text{-}Kfs}$) in spherulites. Fractionations greater than 1‰ are indeed preserved at all positions within the analyzed spherulites, and fractionations increase systematically toward spherulite rims. The fractionations indicate nucleation temperatures and a growth interval that is largely consistent with past experiments and advection-diffusion models. By estimating the temperatures when growth begins and ends, I also constrain growth rates over the crystallization interval.

2. Methods and Results

Spherulites and phenocrysts were extracted from sample Y24, a fist-sized block of obsidian collected from an outcrop near the eastern flow front of Pitchstone Plateau lava flow, Yellowstone Caldera (supporting information Figure S2). Pitchstone Plateau is a high silica rhyolitic obsidian (~77 wt % SiO_2) that was emplaced at 79 ± 10 kya [*Christiansen et al.*, 2007]. It is the largest of the Central Plateau Member rhyolites, with an eruptive volume of ~70 km^3 and flowed up to 15 km from the vent. It is important to note that sample Y24 was also the target sample for advection-diffusion modeling of trace-element gradients outside of spherulites by *Befus et al.* [2015]. Thus, the new oxygen isotope thermometry results can be directly compared to the model results from that study.

Spherulites comprise a small volume percent of the obsidian (<15%) and occur as 400 to 8000 μm diameter, near-spherical ellipsoids. From that population, a group of four similar spherulites was analyzed. These chosen spherulites are representative of spherulites in other obsidian lavas throughout Yellowstone and may be similar to those in other effusive rhyolitic systems. The spherulites ranged from 2000 to 3500 μm in diameter and were internally composed of radiating, elongate, intergrown alkali feldspar and quartz (Figure 2). The crystals appear fresh and unaltered. The crystals radiate outward from central nuclei, which are often phenocrysts of quartz or alkali feldspar. Alkali feldspar in the spherulites is compositionally $Or_{34\pm6}Ab_{64\pm6}$ and does not systematically change in composition with position in the spherulite. Spherulitic alkali feldspar is significantly more sodic than the alkali feldspar phenocrysts from Pitchstone Plateau ($Or_{50\pm2}Ab_{47\pm2}$).

The oxygen isotope compositions of spherulitic and phenocrystic quartz and alkali feldspar were analyzed using the CAMECA IMS 1280 hosted in the Wisconsin Secondary Ion Mass Spectrometer (WiscSIMS)

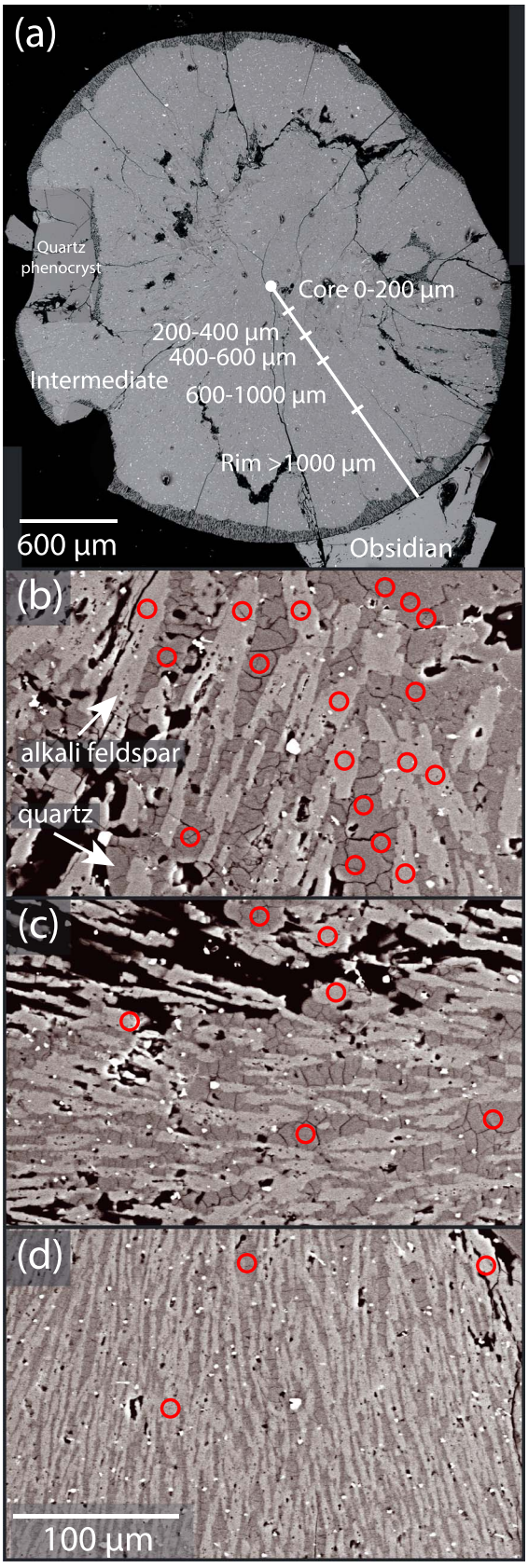

national facility for stable isotope geochemistry at University of Wisconsin-Madison. Data were collected from 8 µm diameter spots. For additional sample preparation and analytical techniques please refer to the online supporting information.

Crystal size systematically decreases approaching spherulite rims in all four targeted spherulites, as is commonly observed in spherulites [e.g., *Gardner et al.,* 2012]. Because of the complex, intergrown crystalline structure, the length of individual crystals is difficult to resolve with confidence. Crystal width, however, can be determined with certainty. Individual crystals within the spherulite cores range from 3 to 200 µm wide, which decreases to 3 to 50 µm in the middle portions, and finally to 2 to 15 µm width at the rims. Analyses were restricted to crystals wider than the ~8 µm diameter analytical spot to ensure that the targets were analyzed with confidence. That approach limited the ability to measure oxygen isotopes in crystals close to the spherulite rims, but some measurements were successfully performed on crystals >1000 µm from the cores.

I organize the analyses into "groups" based on their position relative to the center of the spherulites. I group analyses from the central 200 µm of the spherulites as "Core" and "Rim" as areas >1000 µm from the center (Figure 2). Between those end-members, I define three "Intermediate" groupings at 200–400 µm, 400–600 µm, and 600–1000 µm, respectively. The absolute positions of the five group boundaries are subjective but were chosen to distribute the analyses into statistically significant parcels for $\delta^{18}O$ and $\Delta^{18}O_{Qtz\text{-}Kfs}$ comparisons. Because crystal width decreased toward the rims, fewer analyses

Figure 2. (a) Backscattered scanning electron microscope image of a spherulite in a glassy obsidian matrix. Bin distances used to categorize the data are shown. (b–d) Magnified views of the internal texture of spherulites composed of radiating quartz (dark gray) and alkali feldspar (light gray), which are also labeled in Figure 2b. Void space is black. Fe-Ti oxides are bright. Figure 2b shows core texture; Figure 2c and Figure 2d show gradual crystal fining with distance through the spherulite interior. Red circles represent the location of ~8 µm analytical spots in those domains.

Table 1. Oxygen Isotope Measurements and Temperature Estimates From Quartz and Alkali Feldspar in Spherulites[a]

Position	Distance From Core (μm)	δ^{18}O Quartz (‰)	*n*	δ^{18}O Alkali Feldspar (‰)	*n*	$\Delta^{18}O_{Qtz\text{-}Kfs}$ (‰)	Temperature (°C)
Phenocrysts	n.a.	4.9 (0.4)	4	4.3 (0.4)	9	0.6 (0.7)	950 (383)
Core	0 to 200	5.0 (0.3)	31	3.7 (0.4)	24	1.3 (0.7)	578 (160)
Intermediate 1	200 to 400	5.1 (0.3)	9	3.7 (0.3)	9	1.5 (0.6)	534 (128)
Intermediate 2	400 to 600	5.2 (0.5)	9	3.5 (0.4)	4	1.6 (0.8)	489 (142)
Intermediate 3	600 to 1000	5.1 (0.4)	10	3.2 (0.7)	5	1.9 (1.1)	436 (140)
Rims	>1000	5.6 (0.3)	10	2.7 (0.9)	2	2.9 (1.1)	301 (88)

[a]Analyses by WiscSIMS. Values reported are averages of *n* samples. Values in parentheses represent 1σ standard deviation of the populations.

were possible at spherulite rims. Accordingly, the most distal intermediate and rim domains required more radial space to account for the fewer analyses in those areas.

Quartz and alkali feldspar phenocrysts that act as nuclei, or are embedded within the spherulites, have δ^{18}O values of 4.9 ± 0.4‰ and 4.3 ± 0.4‰, respectively (Table 1 and Figure 3a). In the spherulites, quartz crystals in the cores have δ^{18}O values of 5.0 ± 0.3‰. At interior positions with increasing distance, quartz δ^{18}O are fairly constant at 5.1 ± 0.3‰, 5.2 ± 0.5‰, and 5.1 ± 0.4‰, which increases to 5.6 ± 0.3‰ in distal spherulite rims. Alkali feldspar δ^{18}O values average 3.7 ± 0.4‰ in spherulite cores. δ^{18}O values drop progressively toward spherulite rims and reach to 2.7 ± 0.9‰ in the most distal analyses. The errors reported for δ^{18}O are the 1σ standard deviations of the groupings, which are larger than the analytical uncertainty of each spot (supporting information Table S1). Measured $\Delta^{18}O_{Qtz\text{-}Kfs}$ in phenocrysts is 0.6 ± 0.7‰, whereas spherulite cores have $\Delta^{18}O_{Qtz\text{-}Kfs}$ of 1.3 ± 0.7‰, which increases to 1.6 ± 0.8‰ near the middle portions of transects and to 2.9 ± 1.1‰ at the spherulite rims (Figure 3b). Although relatively large, the errors on $\Delta^{18}O_{Qtz\text{-}Kfs}$ are the propagated 1σ standard deviations of the quartz and alkali feldspar groups and thus fully encompass analytical uncertainty.

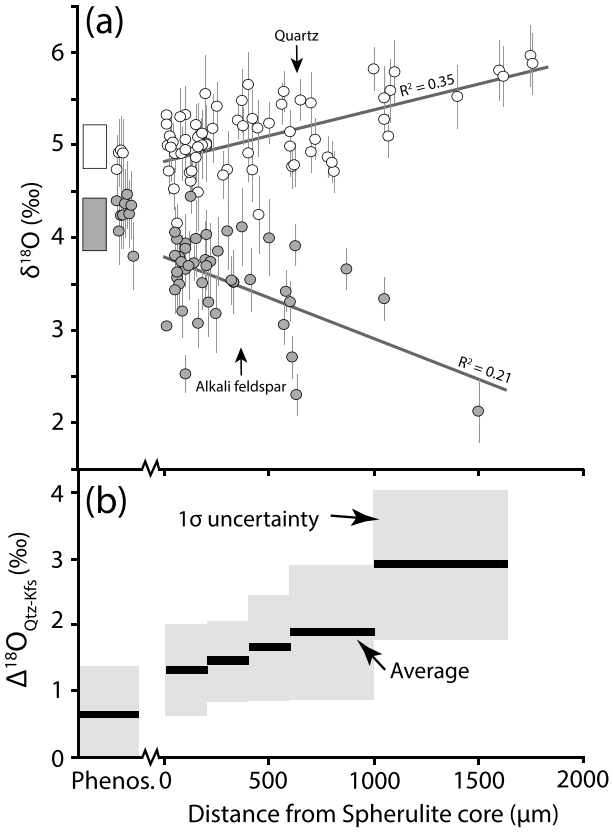

Figure 3. (a) Oxygen isotope compositions of quartz and alkali feldspar shown by white and gray symbols, respectively. Gray lines are linear regressions that highlight the systematic change in δ^{18}O with distance from the core. Gray and white boxes represent previously published ranges in δ^{18}O for quartz and alkali feldspar from Central Plateau Member rhyolites [*Bindeman and Valley*, 2001; *Christiansen et al.*, 2007; *Watts et al.*, 2012]. (b) The fractionation between quartz and alkali feldspar increases with distance from spherulite cores. Black rectangles are averages values, and gray boxes represent 1σ standard deviation of the grouped populations.

Oxygen isotope compositions in quartz and alkali feldspar progressively change with distance from the spherulite cores, such that $\Delta^{18}O_{Qtz\text{-}Kfs}$ systematically increases from core to rim (Figure 3). Before the fractionations can be used for thermometry there must be convincing evidence that the measured oxygen isotope values preserve equilibrium exchange and were unaltered during cooling. I contend that the oxygen isotope record in these spherulites can indeed be used for thermometry based on the following lines of evidence. First, the obsidian hand sample and hosted spherulites appear fresh and show no signs of alteration. Second, the quartz and alkali feldspar in the spherulites are intimately intergrown, demonstrating synchronous crystallization. Finally, volcanic rocks typically retain original isotopic compositions because they cool rapidly [*Chacko et al.*, 2001], which produces high closure

temperatures for diffusive exchange [*Dodson*, 1973]. The closure temperature of oxygen isotope exchange in spherulites is dependent on the thermal history of the host lava, oxygen diffusivity in quartz and alkali feldspar, and grain size. Each of those variables is constrained, so the approximate closure temperature can be estimated [e.g., *Dodson*, 1973]. Pitchstone Plateau is a large-volume, thick lava but likely cooled in less than a few tens of years, especially the upper surface from which the sample was collected. Numerical models and differential scanning calorimetry measurements suggest the sample cooled at ~$10^{-5.2 \pm 0.3}$ °C s^{-1} [*Befus et al.*, 2015]. Oxygen diffusivity in quartz and alkali feldspar is known from experiments [*Farver*, 2010; *Valley*, 2001]. Using those constraints, the closure temperature of oxygen diffusion in spherulites is greater than or equal to magmatic temperatures, which are estimated to have been 720–790°C [*Vazquez et al.*, 2009; *Befus,* 2014; *Stelten et al.*, 2015]. Spherulite crystallization occurred at even cooler temperatures below the glass transition temperature (600–700°C) because spherulites do not deflect flow bands [*Befus et al.*, 2015]. In summary, oxygen was not modified by diffusion, and $\Delta^{18}O_{Qtz\text{-}Kfs}$ can indeed be used for oxygen isotope thermometry.

3. Discussion

The quartz-alkali feldspar fractionation factor is $\alpha_{Qtz\text{-}Kfs} = 0.95$, which is the combination of the $\alpha_{Qtz\text{-}calcite}$ and $\alpha_{albite\text{-}calcite}$ values established in the calcite exchange experiments of *Clayton et al.* [1989]. That fractionation factor has been replicated by other experimental and empirical techniques and appears robust [*Bottinga and Javoy*, 1973; *Zheng*, 1993]. Alkali feldspar can be freely interchanged with albite because the Na-K exchange in feldspar has no effect on fractionation [*Zheng*, 1993; *Chacko et al.*, 2001]. Oxygen isotope fractionation between quartz and alkali feldspar during high temperature crystallization is low compared to other mineral pairs, such as magnetite or zircon [*Zheng*, 1993; *Chacko et al.*, 2001]. Despite this, $\Delta^{18}O_{Qtz\text{-}Kfs}$ is about 1‰ at the estimated eruption temperature of Pitchstone Plateau and increases systematically to ~3‰ at 300°C (Figure 1).

Phenocrysts typically occur in or near the center of the spherulites; hence, it is important to first discuss conditions prior to spherulite formation. Quartz and alkali feldspar phenocrysts crystallized at magmatic temperatures within the Pitchstone Plateau magma chamber. Indeed, the $\Delta^{18}O_{Qtz\text{-}Kfs}$ between those phenocrysts is 0.6 ± 0.7‰, which aligns with expected fractionation for high temperature crystallization. Fractionation in these phenocrysts provides marginal temperature information, but oxygen isotope compositions in quartz and alkali feldspar have been used as a powerful petrologic indicator of magma genesis and evolution in the Yellowstone-Snake River Plain magmatic system [*Hildreth et al.*, 1991; *Bindeman and Valley*, 2000, 2001; *Watts et al.,* 2011]. The new $\delta^{18}O$ values in phenocrysts from Pitchstone Plateau are identical to previously published ranges for quartz (4.8 to 5.2‰) and alkali feldspar (3.8 to 4.4‰) from Pitchstone Plateau and other Central Plateau Member rhyolites, including West Yellowstone, Aster Creek, and Summit Lake [*Bindeman and Valley*, 2001; *Christiansen et al.*, 2007; *Watts et al.,* 2012] (Figure 3a). Importantly, the small, consistent fractionations in Pitchstone Plateau and those other Central Plateau Member rhyolites indicate a return to equilibrium isotopic processes in the magmatic system following the disruption caused by the caldera-forming Lava Creek supereruption [*Hildreth et al.*, 1991; *Bindeman and Valley*, 2000, 2001].

Oxygen isotope compositions vary systematically with position within the spherulites. $\delta^{18}O$ values in quartz increase toward the spherulite rims, whereas $\delta^{18}O$ values in alkali feldspar gradually decrease (Figure 3a). Accordingly $\Delta^{18}O_{Qtz\text{-}Kfs}$ increases with distance from cores. $\delta^{18}O$ values in spherulite cores likely capture nucleation conditions, whereas $\delta^{18}O$ values in spherulite rims likely records conditions when spherulite growth ceased. The fractionation of quartz and alkali feldspar in spherulite cores is 1.31 ± 0.68‰, which is significantly greater than observed in phenocrysts. The spherulite core $\Delta^{18}O_{Qtz\text{-}Kfs}$ corresponds to a temperature of 578 ± 160°C. Fractionation steadily increases through the interior of the spherulites until it reaches 2.9 ± 1.1‰ near the rims, and consequently, crystallization continued until 301 ± 88°C (Figure 4).

Oxygen isotope measurements in spherulites provide a new technique for assessing the natural crystallization kinetics of rhyolitic melts. Based on water-saturated phase equilibria constraints, the upper boundary of joint crystallization of quartz and sanidine in the Pitchstone Plateau lava with ~0.1 wt % H_2O is estimated to be 800 ± 20°C [*Befus,* 2014]. If true, then spherulite nucleation occurs when the melt is undercooled by 100–300°C (Figure 4). Importantly, the entire interval of spherulite growth is predicted to occur at or below the glass transition temperature (600 to 700°C), such that crystallization occurs from solid glass [*Giordano et al.,* 2008]. Spherulite growth continues until the melt is undercooled by 400–600°C. At larger ΔT, crystallization of the glass

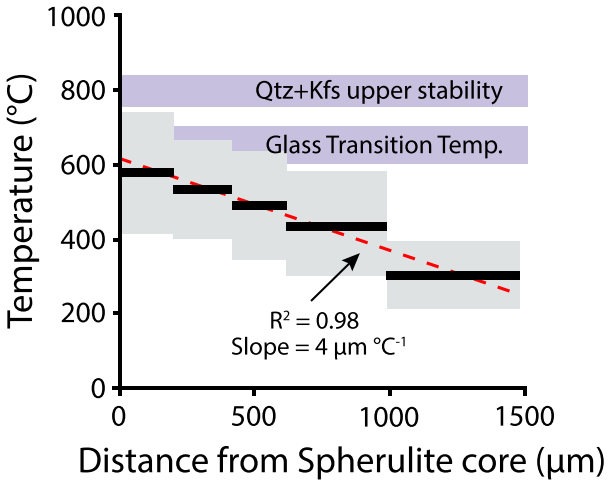

Figure 4. Oxygen isotope thermometry indicates spherulite cores crystallized at ~600°C, and growth continued to ~300°C. Black rectangles are averages values, and gray boxes represent 1σ standard deviation of the groups. Growth occurs below the liquidus stability of coprecipitation of quartz and alkali feldspar from *Befus* [2014] (used to calculate undercooling) and the glass transition temperature [*Giordano et al.,* 2008]. The red dashed line is a linear regression through the data with an R^2 of 0.98. The slope of that line is the spherulite growth rate (4 μm°C^{-1}).

is likely prohibited by the high viscosity and sluggish diffusivities of critical elements for crystal growth such as Si and Al [*Zhang et al.,* 2010].

The uncertainties in oxygen isotope geothermometry limit ΔT estimates to sizable ranges. The estimates are consistent with experiments that performed spherulite growth at ΔT ranging from 100 to 400°C [*Lofgren*, 1974; *Fenn*, 1977; *Kirkpatrick et al.*, 1979; *Baker and Freda*, 2001; *Castro et al.*, 2009]. The $\Delta^{18}O_{Qtz\text{-}Kfs}$ temperature estimates are also comparable with constraints inferred from advection-diffusion modeling of incompatible constituent profiles surrounding spherulites in the same sample from Pitchstone Plateau [*Befus et al.*, 2015]. Based on those models, spherulites were interpreted to nucleate between 700 and 550°C, and growth continued until the lava cooled below ~400°C. Average temperatures from $\Delta_{Qtz\text{-}Kfs}$ are slightly below those estimates but are remarkably similar.

Lastly, it is important to emphasize that the in situ oxygen isotope analyses can be used to track the crystallization progression as a function of temperature (and possibly time), which has previously only been possible in a controlled laboratory environment (Figure 4). Crystal growth per degree cooling is simply the radial distance of spherulite growth divided by the difference in average temperature across that interval. Thus, the slope of a linear regression though the data provides the growth rate (Figure 4). The slope of that regression yields a near constant growth rate of 4 μm°C^{-1}. The regression has an R^2 of 0.98, demonstrating that "best fit" rate is consistent over the entire interval of growth. The uncertainty of that growth rate ranges from 2 μm°C^{-1} to 22 μm°C^{-1}, using the slope of the steepest and shallowest possible lines that remain within the temperature uncertainties (e.g., gray domains in Figure 4). Growth rates are often cast per unit time. Hence, a conversion of temperature to time would be required to directly compare the natural crystallization kinetics with those determined experimentally. Differential scanning calorimetry and advection-diffusion modeling of diffusion profiles surrounding spherulites suggest that sample Y24 from Pitchstone Plateau cooled at ~$10^{-5.2\pm0.3}$ °C s^{-1} [*Befus et al.*, 2015]. Assuming that cooling rate, the best fit for spherulite growth was approximately 0.1 μm h^{-1} and did not significantly vary with decreasing temperature.

The new estimate for spherulite growth is similar to the slower growth rates determined from experiments but is largely similar to results from advection-diffusion modeling [*Fenn*, 1977; *Swanson*, 1977; *Baker and Freda*, 2001; *Castro et al.*, 2009; *Arzilli et al.*, 2015; *Befus et al.*, 2015]. Much of the discrepancy between the new rates and the faster rates determined from past experiments is simply a result of dissimilar materials. Sample Y24 is high silica rhyolite with 0.1 wt % H_2O, whereas a number of the faster experimental growth rates were calculated using water-saturated rhyolitic and trachytic melts, which have lower melt viscosities and faster element diffusivities [e.g., *Fenn*, 1977; *Baker and Freda*, 2001; *Arzilli et al.*, 2015]. Advection-diffusion modeling of spherulite growth is interpreted to demonstrate that an exponentially decreasing growth law best describes spherulite growth, but constant and linearly decreasing growth is also permissible [*Gardner et al.*, 2012; *Befus et al.*, 2015]. It is important to note that my estimate of constant growth is based upon averages for the "grouped" intervals. It is possible that variations in growth rate could be obscured by the coarse temperature uncertainties. Resolution on growth style could be improved in the future with oxygen isotope measurements performed at higher spatial resolution in core and distal positions, which would be more sensitive to differences in growth rates.

In conclusion, oxygen isotope compositions in quartz and alkali feldspar in spherulites provide a novel, in situ measure of crystallization kinetics in rhyolite melts. The technique also provides the first natural measure of the crystal growth rates at subsolidus conditions. The results support and supplement past advection-diffusion models and experiments regarding crystallization kinetics, including nucleation temperature, crystallization temperature interval, and spherulite growth rates. It is remarkable that such extensive temperature-crystallization history can be extracted from spherulites within single obsidian samples. Because spherulites are common features in glassy volcanic rocks, including rhyolitic lavas and welded ignimbrites, this technique can be used to extract crystallization and thermal information from many other volcanic systems worldwide.

Acknowledgments

All supporting data are included in supporting information Table S1. Thoughtful reviews by Ed Marshall, Huaiwei Ni, Kouki Kitajima, and Stephanie Grocke improved this manuscript. I additionally thank Kouki Kitajima, John Valley, and Noriko Kita for help with the WiscSIMS analyses and the grant from National Science Foundation (EAR-1355590) that supports that facility. This research was also made possible by a grant from the National Science Foundation to James E. Gardner (EAR-1049829) and a National Park Service research permit (YELL-05678).

References

Arzilli, F., L. Mancini, M. Voltolini, M. R. Cicconi, S. Mohammadi, G. Giuli, D. Mainprice, E. Paris, F. Barou, and M. R. Carroll (2015), Near-liquidus growth of feldspar spherulites in trachytic melts: 3D morphologies and implications in crystallization mechanisms, *Lithos*, *216–217*, 93–105.

Baker, D. R., and A. Freda (2001), Eutectic crystallization in the undercooled Orthoclase-Quartz-H2O system: Experiments and simulations, *Eur. J. Mineral.*, *13*(3), 453–466, doi:10.1127/0935-1221/2001/0013-0453.

Befus, K. S., J. Watkins, J. E. Gardner, D. Richard, K. M. Befus, N. R. Miller, and D. B. Dingwell (2015), Spherulites as in situ recorders of thermal history in lava flows, *Geology*, *43*(7), 647–650, doi:10.1130/G36639.1.

Befus, K. S. (2014), Storage, ascent, and emplacement of rhyolite lavas, Dissertation, Univ. of Texas at Austin, Austin, Tex.

Bindeman, I. N., and J. W. Valley (2000), Formation of low-δ18O rhyolites after caldera collapse at Yellowstone, Wyoming, USA, *Geology*, *28*(8), 719–722, doi:10.1130/0091-7613(2000)28<719:FOLRAC>2.0.CO;2.

Bindeman, I. N., and J. W. Valley (2001), Low-δ18O Rhyolites from Yellowstone: Magmatic evolution based on analyses of zircons and individual phenocrysts, *J. Petrol.*, *42*(8), 1491–1517, doi:10.1093/petrology/42.8.1491.

Bottinga, Y., and M. Javoy (1973), Comments on oxygen isotope geothermometry, *Earth Planet. Sci. Lett.*, *20*(2), 250–265, doi:10.1016/0012-821X(73)90165-9.

Breitkreuz, C. (2013), Spherulites and lithophysae—200 years of investigation on high-temperature crystallization domains in silica-rich volcanic rocks, *Bull. Volcanol.*, *75*, 1–16.

Cashman, K. V. (1990), Textural constraints on the kinetics of crystallization of igneous rocks, *Rev. Mineral. Geochem.*, *24*(1), 259–314.

Cashman, K. V. (1992), Groundmass crystallization of Mount St. Helens dacite, 1980–1986: A tool for interpreting shallow magmatic processes, *Contrib. Mineral. Petrol.*, *109*(4), 431–449, doi:10.1007/BF00306547.

Cashman, K. V., and B. D. Marsh (1988), Crystal size distribution (CSD) in rocks and the kinetics and dynamics of crystallization II: Makaopuhi lava lake, *Contrib. Mineral. Petrol.*, *99*(3), 292–305, doi:10.1007/BF00375363.

Castro, J. M., P. Beck, H. Tuffen, A. R. L. Nichols, D. B. Dingwell, and M. C. Martin (2008), Timescales of spherulite crystallization in obsidian inferred from water concentration profiles, *Am. Mineral.*, *93*(11–12), 1816–1822, doi:10.2138/am.2008.2904.

Castro, J. M., E. Cottrell, H. Tuffen, A. V. Logan, and K. A. Kelley (2009), Spherulite crystallization induces Fe-redox redistribution in silicic melt, *Chem. Geol.*, *268*(3–4), 272–280, doi:10.1016/j.chemgeo.2009.09.006.

Chacko, T., D. R. Cole, and J. Horita (2001), Equilibrium oxygen, hydrogen and carbon isotope fractionation factors applicable to geologic systems, *Rev. Mineral. Geochem.*, *43*(1), 1–81, doi:10.2138/gsrmg.43.1.1.

Christiansen, R. L., J. B. Lowenstern, R. B. Smith, H. Heasler, L. A. Morgan, M. Nathenson, L. G. Mastin, L. J. P. Muffler, and J. E. Robinson (2007), Preliminary assessment of volcanic and hydrothermal hazards in Yellowstone National Park and Vicinity, *U.S. Geol. Surv. Open File Rep., 2007-1071*, 98 p.

Clayton, R. N., J. R. Goldsmith, and T. K. Mayeda (1989), Oxygen isotope fractionation in quartz, albite, anorthite and calcite, *Geochim. Cosmochim. Acta*, *53*(3), 725–733.

Cross, W. (1891), Constitution and origin of spherulites in acid eruptive rocks, *Philos. Soc. Washington*, *11*, 411–449.

Dodson, M. H. (1973), Closure temperature in cooling geochronological and petrological systems, *Contrib. Mineral. Petrol.*, *40*(3), 259–274.

Farver, J. R. (2010), Oxygen and hydrogen diffusion in minerals, *Rev. Mineral. Geochem.*, *72*(1), 447–507.

Fenn, P. M. (1977), The nucleation and growth of alkali feldspars from hydrous melts, *Can. Mineral.*, *15*(2), 135–161.

Gardner, J. E., K. S. Befus, J. Watkins, M. Hesse, and N. Miller (2012), Compositional gradients surrounding spherulites in obsidian and their relationship to spherulite growth and lava cooling, *Bull. Volcanol.*, *74*(8), 1865–1879, doi:10.1007/s00445-012-0642-9.

Giordano, D., J. K. Russelll, and D. B. Dingwell (2008), Viscosity of magmatic liquids: A model, *Earth Planet. Sci. Lett.*, *271*, 123–134.

Hammer, J. E., and M. J. Rutherford (2002), An experimental study of the kinetics of decompression-induced crystallization in silicic melt, *J. Geophys. Res.*, *107*(B1), 2021, doi:10.1029/2001JB000281.

Hildreth, W., A. N. Halliday, and R. L. Christiansen (1991), Isotopic and chemical evidence concerning the genesis and contamination of basaltic and rhyolitic magma beneath the Yellowstone Plateau Volcanic Field, *J. Petrol.*, *32*(1), 63–138, doi:10.1093/petrology/32.1.63.

Keith, H. D., and F. J. Padden (1963), A phenomenological theory of spherulitic crystallization, *J. Appl. Phys.*, *34*, 2409–2421.

Keith, H. D., and F. J. Padden (1964), Spherulitic Crystallization from the Melt. I. Fractionation and impurity segregation and their influence on crystalline morphology, *J. Appl. Phys.*, *35*, 1270–1285.

Kirkpatrick, R. J. (1977), Nucleation and growth of plagioclase, Makaopuhi and Alae lava lakes, Kilauea Volcano, Hawaii, *Geol. Soc. Am. Bull.*, *88*(1), 78–84, doi:10.1130/0016-7606(1977)88<78:NAGOPM>2.0.CO;2.

Kirkpatrick, R. J., L. Klein, D. R. Uhlmann, and J. F. Hays (1979), Rates and processes of crystal growth in the system anorthite-albite, *J. Geophys. Res.*, *84*(B7), 3671–3676, doi:10.1029/JB084iB07p03671.

Lofgren, G. (1971a), Experimentally produced devitrification textures in natural rhyolitic glass, *Geol. Soc. Am. Bull.*, *82*(1), 111–124, doi:10.1130/0016-7606(1971)82[111:EPDTIN]2.0.CO;2.

Lofgren, G. (1971b), Spherulitic textures in glassy and crystalline rocks, *J. Geophys. Res.*, *76*(23), 5635–5648, doi:10.1029/JB076i023p05635.

Lofgren, G. (1974), An experimental study of plagioclase crystal morphology; isothermal crystallization, *Am. J. Sci.*, *274*(3), 243–273, doi:10.2475/ajs.274.3.243.

Marsh, B. D. (1988), Crystal size distribution (CSD) in rocks and the kinetics and dynamics of crystallization, *Contrib. Mineral. Petrol.*, *99*(3), 277–291, doi:10.1007/BF00375362.

Matsuhisa, Y., J. R. Goldsmith, and R. N. Clayton (1979), Oxygen isotopic fractionation in the system quartz-albite-anorthite-water, *Geochim. Cosmochim. Acta*, *43*(7), 1131–1140, doi:10.1016/0016-7037(79)90099-1.

Matthews, A. (1994), Oxygen isotope geothermometers for metamorphic rocks, *J. Metamorph. Geol.*, *12*(3), 211–219, doi:10.1111/j.1525-1314.1994.tb00017.x.

Seaman, S. J., M. D. Dyar, and N. Marinkovic (2009), The effects of heterogeneity in magma water concentration on the development of flow banding and spherulites in rhyolitic lava, *J. Volcanol. Geotherm. Res.*, *183*(3–4), 157–169, doi:10.1016/j.jvolgeores.2009.03.001.

Stelten, M. E., K. M. Cooper, J. A. Vazquez, A. T. Calvert, and J. J. G. Glessner (2015), Mechanisms and timescales of generating eruptible rhyolitic magmas at Yellowstone Caldera from Zircon and Sanidine Geochronology and Geochemistry, *J. Petrol.*, *56*, 1607–1642.

Swanson, S. E. (1977), Relation of nucleation and crystal-growth rate to the development of granitic textures, *Am. Mineral.*, *62*(9–10), 966–978.

Tuttle, O. F., and N. L. Bowen (1958), Origin of granite in the light of experimental studies in the system naalsi3o8–kalsi3o8–sio2–h2o, *Geol. Soc. Am. Mem.*, *74*, 1–146, doi:10.1130/MEM74-p1.

Valley, J. W. (2001), Stable isotope thermometry at high temperatures, *Rev. Mineral. Geochem.*, *43*(1), 365–413, doi:10.2138/gsrmg.43.1.365.

Vazquez, J. A., S. F. Kyriazis, M. R. Reid, R. C. Sehler, and F. C. Ramos (2009), Thermochemical evolution of young rhyolites at Yellowstone: Evidence for a cooling but periodically replenished postcaldera magma reservoir, *J. Volcanol. Geotherm. Res.*, *188*(1–3), 186–196, doi:10.1016/j.jvolgeores.2008.11.030.

von Aulock, F. W., A. R. L. Nichols, B. M. Kennedy, and C. Oze (2013), Timescales of texture development in a cooling lava dome, *Geochim. Cosmochim. Acta*, *114*, 72–80.

Watkins, J., M. Manga, C. Huber, and M. Martin (2009), Diffusion-controlled spherulite growth in obsidian inferred from H_2O concentration profiles, *Contrib. Mineral. Petrol.*, *157*(2), 163–172, doi:10.1007/s00410-008-0327-8.

Watts, K. E., I. N. Bindeman, and A. K. Schmitt (2011), Large-volume rhyolite genesis in caldera complexes of the Snake River Plain: Insights from the Kilgore Tuff of the Heise Volcanic Field, Idaho, with comparison to Yellowstone and Bruneau-Jarbridge Rhyolites, *J. Petrol.*, *52*, 857–890.

Watts, K. E., I. N. Bindeman, and A. K. Schmitt (2012), Crystal scale anatomy of a dying supervolcano: An isotope and geochronology study of individual phenocrysts from voluminous rhyolites of the Yellowstone caldera, *Contrib. Mineral. Petrol.*, *164*, 45–67.

Yoder, H. S., and C. E. Tilley (1962), Origin of Basalt Magmas: An experimental study of natural and synthetic rock systems, *J. Petrol.*, *3*(3), 342–532, doi:10.1093/petrology/3.3.342.

Zhang, Y., H. Ni, and Y. Chen (2010), Diffusion data in silicate melts, *Rev. Mineral. Geochem.*, *72*, 311–408.

Zheng, Y.-F. (1993), Calculation of oxygen isotope fractionation in anhydrous silicate minerals, *Geochim. Cosmochim. Acta*, *57*, 1079–1091, doi:10.1016/0016-7037(93)90042-U.